Reconstruction of the murine extrahepatic biliary tree using primary human extrahepatic cholangiocyte organoids.

Fotios Sampaziotis[1,2,3], Alexander W Justin[4], Olivia C. Tysoe[1,2], Stephen Sawiak[5†], Edmund M Godfrey[6†], Sara S Upponi[6†], Richard L. Gieseck III[7], Miguel Cardoso de Brito[1,2], Natalie Lie Berntsen[8], María J Gómez-Vázquez[9], Daniel Ortmann[1,2], Loukia Yiangou[1,10,11], Alexander Ross[1,12,13], Johannes Bargehr[1,10,11,14], Alessandro Bertero[1,2], Mariëlle CF Zonneveld[1], Marianne T Pedersen[15], Matthias Pawlowski[1], Laura Valestrand[8], Pedro Madrigal[1,16], Nikitas Georgakopoulos[2], Negar Pirmadjid[2], Gregor M Skeldon[17,18], John Casey[19], Wenmiao Shu[17,18], Paulina M Materek[20], Kirsten E Snijders[1], Stephanie E Brown[1,2], Casey A Rimland[1,2,7,21], Ingrid Simonic[22], Susan E Davies[23], Kim B Jensen[15], Matthias Zilbauer[10,12,13], William TH Gelson[3], Graeme J. Alexander[11], Sanjay Sinha[1,14], Nicholas RF Hannan[24,25], Thomas A Wynn[7], Tom H Karlsen[8], Espen Melum[8], Athina E. Markaki[4], Kourosh Saeb-Parsy[2*], Ludovic Vallier[1,2,10,16*]

[1]Wellcome Trust-Medical Research Council Stem Cell Institute, Cambridge Stem Cell Institute, Anne McLaren Laboratory, University of Cambridge, Cambridge, UK

[2]Department of Surgery, University of Cambridge and NIHR Cambridge Biomedical Research Centre, Cambridge, UK

[3]Department of Hepatology, Cambridge University Hospitals NHS Foundation Trust, Cambridge, UK

[4]Department of Engineering, University of Cambridge, Cambridge, UK

[5]Department of Clinical Neurosciences, University of Cambridge, Cambridge, UK

[6]Department of Radiology, Cambridge University Hospitals NHS Foundation Trust, Cambridge, UK

[7]Immunopathogenesis Section, Laboratory of Parasitic Diseases, National Institute of Allergy and Infectious Diseases, National Institutes of Health, Bethesda, Maryland, USA

[8]Norwegian PSC Research Center, Department of Transplantation Medicine, Division of Surgery, Inflammatory Diseases and Transplantation, Oslo University Hospital, Rikshospitalet, Oslo.

[9]Cambridge Genomic Services, Department of Pathology, University of Cambridge, Cambridge, UK

[10]Wellcome Trust-Medical Research Council Stem Cell Institute, Cambridge Stem Cell Institute, University of Cambridge, Cambridge, UK

[11]Department of Medicine, School of Clinical Medicine, University of Cambridge, Cambridge, UK.

[12]University Department of Paediatrics, University of Cambridge, Cambridge, UK

[13]Department of Paediatric Gastroenterology, Hepatology and Nutrition, Cambridge University Hospitals NHS Foundation Trust, Cambridge, UK

[14]Division of Cardiovascular Medicine, University of Cambridge, Cambridge, UK

[15]Biotech Research and Innovation Centre (BRIC), University of Copenhagen, Copenhagen, Denmark

[16]Wellcome Trust Sanger Institute, Hinxton, UK

[17]School of Engineering and Physical Sciences, Heriot-Watt University, United Kingdom

[18]Department of Biomedical Engineering, University of Strathclyde, United Kingdom

[19]Department of Surgery, University of Edinburgh, Edinburgh Royal Infirmary, Edinburgh, EH16 4SU, United Kingdom

[20]NIHR Cambridge Biomedical Centre (BRC) hIPSCs core facility

[21]University of North Carolina, Chapel Hill School of Medicine, Chapel Hill, North Carolina, USA

[22]Medical Genetics Laboratories, Cambridge University Hospitals NHS Trust, Cambridge, UK

[23]Department of Histopathology, Cambridge University Hospitals NHS Foundation Trust, Cambridge, UK

[24]Center for Biomolecular Sciences, University of Nottingham, UK

[25]Nottingham Digestive Diseases Centre, National Institute for Health Research (NIHR) Nottingham Biomedical Research Centre at the Nottingham University Hospitals NHS Trust and University of Nottingham.

Authorship note: * Kourosh Saeb-Parsy and * Ludovic Vallier contributed equally to this work.

[†]Stephen Sawiak, [†]Edmund Godfrey and [†]Sara Upponi contributed equally to this work.

Correspondence: Ludovic Vallier, Laboratory for Regenerative Medicine, West Forvie Building, Robinson Way, University of Cambridge. Cambridge

CB2 0SZ, United Kingdom. Telephone: 44.1223.747489; Fax: 44.1223.763.350; E-mail: lv225@cam.ac.uk.

Keywords: Cholangiocytes, bile duct, bio-engineering, tissue engineering, organoids, regenerative medicine, cell-based therapy, biliary atresia, PGA scaffold, collagen scaffold, densified collagen

Abstract

The treatment of common bile duct disorders such as biliary atresia or ischemic strictures is restricted by the lack of biliary tissue from healthy donors suitable for surgical reconstruction. Here, we report a novel method for the isolation and propagation of human cholangiocytes from the extrahepatic biliary tree in the form of Extrahepatic Cholangiocyte Organoids (ECOs) for regenerative medicine applications. The resulting ECOs closely resemble primary cholangiocytes in terms of transcriptomic profile and functional properties. We explore the regenerative potential of these organoids *in vivo* and demonstrate that ECOs self organize into bile duct-like tubes expressing biliary markers following transplantation under the kidney capsule of immunocompromised mice. In addition, when seeded on biodegradable scaffolds, ECOs form tissue-like structures retaining biliary characteristics. The resulting bioengineered tissue can reconstruct the gallbladder wall and repair the biliary epithelium following transplantation in a mouse injury model. Furthermore, bioengineered artificial ducts can replace the native common bile duct with no evidence of cholestasis or lumen occlusion. In conclusion, ECOs can successfully reconstruct the biliary tree providing proof-of-principle for organ regeneration using human primary cholangiocytes expanded in vitro.

Disorders of the extrahepatic bile ducts carry considerable morbidity and mortality. Indeed, 70% of pediatric liver transplantations are performed to treat biliary atresia[1], Primary Sclerosing Cholangitis (PSC) alone accounts for 5% of US liver transplantations[2] and biliary complications are the leading cause of graft failure following deceased liver transplantation[3,4]. Treatment options remain limited[5,6] due to the lack of healthy **donor** tissue that can be used to reconstruct and replace diseased bile ducts. In vitro expansion of native cholangiocytes could address this challenge and provide cells suitable for tissue engineering applications such as biliary reconstruction. However, the culture of primary biliary epithelium remains problematic[7]. Here we report a novel method for the isolation and propagation of primary human cholangiocytes from the extrahepatic biliary tree, compatible with regenerative medicine applications. The resulting Extrahepatic Cholangiocyte Organoids (ECOs) express key biliary markers such as Cytokeratin 7 (KRT7 or CK7), Cytokeratin 19 (KRT19 or CK19), Gamma Glutamyl-Transferase (GGT), Cystic fibrosis transmembrane conductance regulator (CFTR) and maintain their functional properties in vitro including Alkaline Phosphatase (ALP), GGT activity and responses to secretin and somatostatin. The potential of ECOs for tissue engineering and clinical applications is further illustrated by their capacity to populate biodegradable scaffolds, organize into a functional biliary epithelium and rescue a murine model of extrahepatic biliary injury (EHBI).

Results

Human extrahepatic cholangiocytes can be propagated as organoids

We first focused on identifying optimal conditions to isolate primary cholangiocytes from the biliary epithelium which forms a monolayer covering the luminal surface of the biliary tree[8]. We tested several approaches for recovering these cells (**Supplementary Fig. 1a**-**c**) and mechanical dissociation by brushing or scraping the bile duct lumen was associated with improved survival compared to enzymatic digestion (**Fig. 1a** and **Supplementary Fig. 1a**). Furthermore, the majority of the resulting cells co-expressed the biliary markers CK7 and CK19 (94.6 ± 2.4%, SD; *n* = 3); while no contamination from mesenchymal cell types was detected (**Supplementary Fig. 1d**). Consequently, mechanical dissociation constitutes the optimal method for harvesting extrahepatic cholangiocytes.

To discern appropriate conditions for the maintenance and propagation of these cells, we optimized our recently established system for 3D culture of human induced pluripotent stem cell-derived intrahepatic cholangiocytes[9,10]. Screening of multiple growth factors known to support expansion of cholangiocytes and epithelial organoids[11,12] (**Supplementary Fig. 1b**,**c**) identified the combination of Epidermal Growth Factor (EGF), R-spondin and Dickkopf-related protein 1 (DKK-1) as sufficient to promoted the growth of primary cholangiocytes into organoids (**Supplementary Fig. 1c**). Due to the paradoxical requirement for both a Wnt potentiator (R-spondin) and an inhibitor (DKK-1), we characterized the canonical and non-canonical/PCP Wnt pathway activity in ECOs. Our results demonstrate higher β-catenin phosphorylation in ECOs compared to cells treated with R-spondin but no DKK-1 (**Supplementary Fig. 1e**,**f**), signifying lower WNT canonical pathway activity in these cells. Furthermore ECOs exhibit higher Rho Kinase activity

compared to cells treated with R-spondin but no DKK-1 (**Supplementary Fig. 1g)**, which could be consistent with enhanced non-canonical/PCP signaling in ECOs. Thus, it is possible that non-canonical Wnt signaling controls ECO expansion marking a notable difference with previous organoid culture conditions[12].

Under these conditions, we derived 8 different ECO lines (**Fig1. a**-**d**, **Supplementary Fig. 2a**-**f**, **Supplementary Fig. 3a**-**e** and **Supplementary Table 1**) from a variety of deceased donors aged from 33 to 77 years. Notably, we obtained similar results by using cholangiocytes isolated from the gallbladder or by harvesting common bile duct cholangiocytes using an Endoscopic Retrograde Cholangio-Pancreatography (ERCP) brush instead of scrapping the lumen (**Supplementary Fig. 2a**,**b**). Consequently, ECOs can be derived from different areas of the extra-hepatic biliary tree and harvested using peri-operative (dissection and scrapping) or minimally invasive (ERCP brushings) approaches.

ECOs maintain key biliary markers and function in culture

The resulting cells were expanded in vitro for prolonged periods of time (**Supplementary Fig. 4a**) while maintaining their genetic stability (**Supplementary Fig 4b**,**c**). Electron microscopy revealed the presence of characteristic ultrastructural features including cilia, microvilli and tight junctions[13] (**Supplementary Fig. 3c**), while QPCR and immunofluorescence (IF) analyses established the expression of key biliary markers such as *KRT7* or *CK7*, *KRT19* or *CK19*, Hepatocyte Nuclear Factor 1 beta (*HNF1B*), *GGT*,

Secretin Receptor (*SCTR*), sodium-dependent bile acid transporter (*ASBT/SLC10A2*), *CFTR* and SRY-box 9 (*SOX9*)[9] (**Fig. 1b**,**c** and **Supplementary Fig. 2c**,**d** and **Supplementary Fig. 3d**,**e)**. Of note, stem cell markers such as *POU5F1* or *OCT4*, *NANOG*, prominin 1 (*PROM1*), leucine rich repeat containing G protein-coupled receptor (*LGR*) *LGR-4/5/6*; markers of non-biliary lineages including albumin (*ALB*), α1-antitrypsin (*SERPINA1* or *A1AT*), keratin 18 (*KRT18*), pancreatic and duodenal homeobox 1 (*PDX1*), insulin (*INS*) and glucagon (*GCG*); and EMT markers (vimentin (*VIM*), snail family transcriptional repressor 1 (*SNAI1*) and S100 calcium binding protein A4 (*S100A4*) were not detected (**Supplementary Fig. 5a**-**c**). On the other hand, 98.1% ± 0.9% (SD; *n* = 3) of the cells co-expressed CK7 and CK19 following 20 passages (**Supplementary Fig. 1d**) thereby confirming the presence of a near homogeneous population of cholangiocytes.

Transcriptomic analyses (**Fig. 1d** and **Supplementary Fig. 6** and **Supplementary Table 2**) revealed that ECOs maintain a stable gene expression profile over multiple passages (Pearson correlation coefficient for Passage 1 (P1) vs. Passage 20 (P20) *r* = 0.99, **Supplementary Fig. 6a**,**b**), express key biliary markers (**Supplementary Fig. 6c**) and cluster closely to freshly isolated cholangiocytes (**Supplementary Fig. 6d**) (Pearson correlation coefficient for Primary Cholangiocytes (PCs) vs. Passage 20 (P20) *r* = 0.92; **Supplementary Fig. 6b**). Gene ontology analyses confirmed enrichment of pathways characteristic for the biliary epithelium (**Supplementary Fig. 6e**). Considered collectively, these results demonstrate that primary cholangiocytes derived from the extrahepatic biliary tree can be expanded in vitro without losing their original characteristics.

We then further characterized ECOs by focusing on their function following long-term culture (20 passages). The biliary epithelium regulates the homeostasis of bile through the transport of ions, water and bile acids[8,14]. The secretory capacity of ECOs was interrogated using Rhodamine-123, a fluorescent substrate for the cholangiocyte surface glycoprotein Multidrug Resistance protein-1 (MDR1)[15,16] (**Fig. 2a**-**c**). Rhodamine-123 accumulated in the ECO lumen only in the absence of the MDR-1 antagonist verapamil, thereby confirming active secretion through MDR-1 (**Fig. 2a**-**c**). Luminal extrusion of bile acids[17] was also demonstrated by showing that the fluorescent bile acid Cholyl-Lysyl-Fluorescein (CLF) was actively exported from ECOs (**Fig. 2d**-**f**). Furthermore, ECO ALP and GGT activity was comparable to freshly plated primary cholangiocytes (**Fig. 2g-h** and **Supplementary Fig. 2e**,**f**). The response of ECOs to secretin and somatostatin was also assessed. Secretin promotes water secretion, distending the bile duct lumen, while somatostatin negates the effects of secretin[18–20]. Accordingly, organoids exposed to secretin increased their diameter compared to untreated controls, while somatostatin inhibited the effect of secretin (**Fig. 2i**-**j**). Our data, therefore, demonstrate that ECOs maintain their functional properties after long term culture.

ECOs self-organize into bile duct like tubes after transplantation

These results prompted us to investigate the potential of ECOs for *in vivo* use, especially regenerative medicine applications. We first characterized the potential of ECOs for *in vivo* engraftment and survival by transplanting cells

under the kidney capsule of NOD.Cg-Prkdc^{scid} Il2rg^{tm1Wjl} (NSG) mice (**Supplementary Fig. 7a**) for 12 weeks[21]. ECOs successfully engrafted forming tubular structures expressing biliary markers such as CK19 (**Supplementary Fig. 7b-d**).

Notably, no tumor formation or markers of differentiation to other lineages were detected (**Supplementary Fig. 7d**). Thus, ECOs appear to maintain their basic characteristics even after prolonged engraftment in vivo under the kidney capsule.

ECO-populated scaffolds reconstruct the gallbladder wall

To assess the potential of ECOs for tissue engineering, we first interrogated their capacity for populating polyglycolic acid (PGA) biodegradable scaffolds commonly used to provide the structural and mechanical support required for tissue reconstruction[22]. Indeed, PGA is one of the most widely used synthetic polymers since it does not induce inflammatory responses in the surrounding tissue; it is biodegradable; and it is more flexible and easier to process compared to natural polymers such as collagen[23]. To facilitate tracking of the cells, ECOs expressing Green Fluorescent Protein (GFP) were generated through viral transduction (**Supplementary Fig. 8**). The resulting cells were seeded on PGA scaffolds, attached to the PGA fibers after 24-48 hours and continued to grow for 4 weeks until the scaffold was confluent (**Fig. 3a-d**). Of note, primary cholangiocytes grown in 2D conditions demonstrated limited expansion potential and failed to reach confluency when seeded on the scaffolds (**Supplementary Fig. 9**), suggesting that the proliferative capacity of

ECOs is crucial for successful scaffold colonization. The populated PGA scaffolds (**Fig. 3b**,**c**), could easily be handled with forceps and divided into smaller pieces with a surgical blade. Furthermore, the cells populating the scaffolds retained expression of biliary markers such as CK7 and CK19 (**Fig. 3e**,**f**), demonstrated no evidence of epithelial–mesenchymal transition (EMT; **Fig. 3e**,**g**) and maintained their functional properties including ALP and GGT activity (**Fig. 3h**,**i**). Therefore, ECOs can populate PGA scaffolds while maintaining their functionality and marker expression thereby providing a bioengineered tissue resembling the biliary epithelium.

We then decided to define the capacity of ECOs to repair the biliary epithelium. For that, we developed a mouse model of extrahepatic biliary injury (EHBI). More specifically, to simulate biliary tree wall defects requiring biliary reconstruction[24], the biliary tree of healthy NSG mice was compromised through a longitudinal incision in the gallbladder wall (**Fig. 4a**). The surgical defect in the gallbladder wall was subsequently repaired by transplanting PGA scaffolds populated with GFP-ECOs into the injured animals (**Fig. 4a**-**g** and **Supplementary Fig. 10a**-**f**). Acellular PGA scaffolds and scaffolds populated with GFP-expressing fibroblasts (**Supplementary Fig. 11a**-**d**) were used as a negative controls. Animals receiving acellular scaffolds died within 24 hours of the operation (**Fig. 4b**) and post-mortem examination revealed yellow pigmentation of the peritoneal cavity and seminal vesicles consistent with bile leak (**Supplementary Fig. 10a**); while all animals in the fibroblast-scaffold group failed to reconstruct their gallbladder which was replaced by fibrotic tissue incompatible with bile transport or storage (**Supplementary Fig. 11e**-**g**). In contrast, animals transplanted with scaffolds containing ECOs survived

for up to 104 days without complications and were culled electively (**Fig. 4b**). Notably, the reconstructed gallbladders in the ECO group were fully remodeled resembling the morphology of their native counterparts (**Fig. 4c** and **Supplementary Fig. 10b**). Histology (**Fig. 4d**), IF and QPCR analyses of the ECO-reconstructed gallbladders (**Fig. 4e** and **Supplementary Fig. 10c,d**) unveiled integration of GFP-positive ECOs expressing biliary markers, such as *KRT19*, *KRT7*, *HNF1B*, *SOX9*, *CFTR* and a human-specific epitope for Ku80 (**Fig. 4e** and **Supplementary Fig. 10c**). Of note, these IF analyses also showed the presence of mouse mesenchymal cells expressing vimentin and endothelial cells expressing CD31 in the reconstructed biliary epithelium suggesting that the scaffold is colonized by endogenous cells after transplantation (**Supplementary Fig. 10c**). Furthermore, we also identified a population of GFP+/vimentin+/CK19- cells, suggesting that ECOs may also contribute to the scaffold stroma *in vivo*; possibly through EMT (**Supplementary Fig. 10c**,**e**). The integrity of the reconstructed gallbladder lumen and its exposure to bile through continuity with the biliary tree were demonstrated using magnetic resonance cholangio-pancreatography (MRCP) imaging prior to removal of the organ and was further confirmed with FITC cholangiograms (**Fig. 4f**,**g** and **Supplementary Fig. 10f** and **Supplementary Video 1**). Post mortem surgical examination and full body magnetic resonance imaging 104 days post transplantation revealed no evidence of tumor formation (**Supplementary Fig. 10f** and **Supplementary Video 2**) while IF analyses revealed no GFP+ cells in the adjacent liver tissue (data not shown). On the contrary, gallbladders reconstituted with fibroblast controls exhibited obliteration of the gallbladder lumen (**Supplementary Fig. 11h**,**i**)

and replacement of the lumen and biliary epithelium by fibroblasts expressing Fibroblast Specific Antigen S100A4 (**Supplementary Fig. 11i-j**). Considered collectively, our findings demonstrate the capacity of ECOs to colonize their physiological niche and regenerate part of the biliary tree without any complications.

Bioengineered bile ducts replace the native mouse bile duct

Reconstruction of the gallbladder wall provided proof-of-principle for the capacity of ECOs to repair the biliary epithelium after injury; however, the majority of extrahepatic bile duct disorders affect the common bile duct (CBD). Therefore, we focused on the generation of a tubular ECO-populated scaffold, which could be used for bile duct replacement surgery. The internal diameter of the mouse CBD is approximately 100μm with a wall thickness of less than 50μm, which precluded the use of a PGA scaffold due to mechanical properties. Instead, we generated densified collagen tubular scaffolds (**Fig. 5a**,**b**) which were populated with GFP-expressing ECOs (**Fig. 5c**-**e**). The use of densified collagen enabled the generation of constructs with an external diameter ranging from 250 to 600μm and adequate strength to maintain a patent lumen (**Fig. 5d**). Notably, the cells populating the collagen scaffolds maintained expression of biliary markers such as *KRT19*, *KRT7*, *HNF1B*, *SOX9* and *CFTR* (**Fig. 5f,g**) and exhibited GGT and ALP enzymatic activity (**Fig. 5h**,**i**). Primary epithelial cells of different origin (human mammary epithelial cells; HMEC) failed to survive and adequately populate densified collagen tubes under the same conditions (**Supplementary Fig. 12a**). Moreover, plated HMECs failed to survive in a 10% (vol/vol) bile solution

(**Supplementary Fig. 12b**), further confirming the unique capacity of ECOs for generating bile resistant bio-engineered bile ducts. Collectively, these results demonstrate the capacity of ECOs for populating tubular densified collagen scaffolds without losing their original characteristics.

We then decided to explore the possibility to replace the native CBD of NGS mice with a bioengineered duct consisting of an ECO-populated densified collagen tube as described above. A mid-portion of the native CBD was removed and an ECO-populated collagen tube was anastomosed end-to-end to the proximal and distal duct remnants (**Fig. 6a**). Fibroblast populated tubes were used as a negative control. Biliary reconstruction was achieved in all animals transplanted with ECO-populated tubes (**Figure 6b,c** and **Supplementary Fig. 13a**-**d**), which were followed up for up to a month post transplantation (**Supplementary Fig. 13d**). Histology and IF and QPCR analyses (**Fig. 6d**-**f** and **Supplementary Fig. 13a**,**b**) revealed a patent lumen, with formation of a biliary epithelium by the transplanted GFP+ cells (**Fig. 6e**,**f** and **Supplementary Fig 13a**,**b**); confirmed the expression of biliary markers, such as *KRT19*, *KRT7*, *HNF1B*, *CFTR*, *SOX9* **(Fig. 6d**,**f** and **Supplementary Fig. 13b**) by the engrafted cells; but also illustrated the presence of mouse stromal and endothelial cells (**Supplementary Fig. 13b**). Moreover, we observed minimal apoptosis and proliferation in the transplanted tubes 1 month after transplantation, confirming the stability and integrity of the reconstituted biliary epithelium (**Supplementary Fig. 13b**,**c**). Lumen patency was further confirmed by Fluorescein Isothiocyanate (FITC) cholangiogram, MRCP and serum cholestasis marker measurements (**Fig. 6g** and **Supplementary Fig. 13e**,**f** and **Supplementary Video 3**). Accordingly

356 animals receiving ECO-populated tubes exhibited no elevation in serum
357 cholestasis markers (Bilirubin, ALP; **Supplementary Fig. 13e**) and a patent
358 lumen on imaging (**Fig. 6g** and **Supplementary Fig. 13f**); while the bio-
359 artificial common bile ducts retained their ALP activity in vivo (**Fig. 6h**).

360 On the contrary, all fibroblast-populated collagen tubes failed due to
361 lumen occlusion (**Fig. 6b**,**c**,**e**-**g** and **Supplementary Fig. 13d**), resulting in
362 high biliary pressures and bile leak through the site of anastomosis (**Fig. 6b**).
363 In conclusion, our results demonstrate the capacity of ECO-populated
364 collagen tubes to replace the native CBD in vivo.

365

366 **Discussion**

367 We have demonstrated that epithelial cells from the extrahepatic biliary tree
368 can be expanded and propagated *in vitro* while maintaining their
369 cholangiocyte transcriptional signature and functional characteristics. In
370 addition, our results show that primary cholangiocytes expanded *in vitro* as
371 organoids have a unique potential for organ regeneration. Indeed, our system
372 provides the first proof-of-principle for the application of regenerative medicine
373 in the context of common bile duct pathology. The capacity to replace a
374 diseased common bile duct with an *in vitro* bio-engineered ECO-tube could
375 have a considerable impact for the management of disorders such as biliary
376 atresia, which constitutes the leading cause for pediatric liver transplantation[1];
377 or ischemic strictures which are one of the most common complications
378 following transplantation[3]. Consequently ECO-populated scaffolds constitute a
379 novel system with high clinical relevance in the field of cholangiopathies.

Studies of the extrahepatic biliary epithelium have been limited by technical challenges in long-term culture and large-scale expansion of primary cholangiocytes. These challenges have so far precluded large scale experiments such as transcriptomic and genome-wide analyses which are urgently needed to better understand bile duct diseases, such as PSC and cholangiocarcinoma. The capacity of ECOs for large scale expansion, could address this challenge. Indeed, we demonstrate that starting from 10^5 extrahepatic cholangiocytes we can generate between 10^{20} – 10^{25} cells after 20 passages. Therefore, ECOs not only represent a novel source of cells for cell-based therapy but also provide a unique model system for studying the physiology and modeling disorders of the extrahepatic biliary tree *in vitro*.

Access to human tissue constitutes a considerable limitation for systems based on primary cells. However, we show that ECOs can be obtained not only from the common bile duct but also from the gallbladder. Gallbladder tissue is easily accessible and routinely discarded following liver transplantation and cholecystectomy, one of the most common surgical procedures performed. Furthermore, in individuals not having surgery the common bile duct can be accessed using minimally invasive procedures, such as endoscopic retrograde cholangio-pancreatography (ERCP) and we demonstrate that cholangiocytes can be obtained through brushings, which are routinely performed to acquire histology specimens. Notably, no morphological or functional differences were observed between organoids obtained with these different methods. Moreover, due to the scalability of our system only a small amount of starting material is required. Finally, recent progress in replacing Matrigel by custom made hydrogels to grow gut

organoids[25] suggest that translating our system from Matrigel to more clinically relevant good manufacturing practice could be feasible. Considered together, these approaches effectively address challenges of tissue availability and open the possibility of autologous as well as allogeneic cell based therapy.

Notably, the derivation of primary hepatic stem cells using an organoid culture system has been reported previously[12]. However, the capacity of the resulting cells to differentiate into functional cholangiocytes and populate the biliary tree *in vivo* remains to be demonstrated. Furthermore, *in vivo* applications of such platforms could be restricted by contaminating stem cells with a capacity to proliferate inappropriately after transplantation and/or differentiate into non-biliary cell types. Despite the association between organoids and adult stem cells[26], we never observed the expression of hepatocyte or pancreatic markers during our experiments either *in vitro* or after transplantation, suggesting that the differentiation capacity of ECOs is limited to their lineage of origin. Moreover, canonical WNT signaling, which is crucial for the expansion of adult stem cell organoids[27] is blocked in our culture conditions through the use of DKK-1 and further studies may be required to fully elucidate the role of R-spondin in our system. Considered together, these observations suggest that our culture system does not include a stem cell population. However, we cannot completely exclude that these cells could represent a biliary progenitor population based on their ability to self-propagate and generate organoids from single cells.

Of note, we have recently established a system for the generation of human pluripotent stem cell-derived cholangiocyte-like cells (CLCs)[9].

However, it is worth underlining that there are considerable differences between ECOs and CLCs. CLCs correspond to intrahepatic cholangiocytes, while ECOs represent extrahepatic biliary epithelium. These two cell types are distinct in terms of embryological origin and disease involvement[14] and therefore the two systems complement each other for studies of the biliary tree. Indeed, CLCs are generated following a natural path of development and maintain fetal characteristics. Therefore, they provide a unique system to study human biliary development and developmental diseases which is not possible using adult cells. However, CLCs may require a period of adjustment and further maturation in vivo, while mature, functional cells, such as ECOs, are required for coping with biliary injury in the acute setting and may be better suited for regenerative medicine applications. Furthermore, although hIPSCs provide a very good source of cells capable of generating almost any tissue, initial derivation/characterization of hIPSC lines remains time consuming; while variability in capacity of differentiation still constitutes a challenge. ECOs can be derived in less than 24 hours with a very high efficiency and can be expanded for multiple passages without losing their original characteristics. Consequently, ECOs and CLCs are comparable in terms of scalability and complementary in terms of applications, with the mature phenotype of ECOs providing a unique advantage for regenerative medicine applications in the context of tissue repair.

In conclusion, our results open up novel avenues for the use of extrahepatic primary biliary tissue as a novel platform for *in vitro* studies, disease modeling and cell based therapy applications.

Accession codes

Accession number for microarray data: E-MTAB-4591.

Data availability statement

The microarray data are open access and available online on ArrayExpress (https://www.ebi.ac.uk/arrayexpress/)

Acknowledgements: This work was funded by ERC starting grant Relieve IMDs (LV, NRFH), the Cambridge Hospitals National Institute for Health Research Biomedical Research Center (LV, NRFH, SaS, FS.), the Evelyn trust (NH) and the EU Fp7 grant TissuGEN (MCDB) and supported in part by the Intramural Research Program of the NIH/NIAID (RLG, CAR). FS has been supported by an Addenbrooke's Charitable Trust Clinical Research Training Fellowship and a joint MRC-Sparks Clinical Research Training Fellowship. AWJ and AEM acknowledge the support from EPSRC (EP/L504920/1) and an Engineering for Clinical Practice Grant from the Department of Engineering, University of Cambridge. JB was supported by a BHF Studentship (Grant FS/13/65/30441).

The authors would like to thank J Skepper, L Carter and the University of Cambridge Advanced Imaging Centre for their help with electron microscopy; E Farnell and the University of Cambridge, Cambridge Genomic Services for their help with microarray data processing and analysis; A Petrunkina and the NIHR Cambridge BRC Cell Phenotyping Hub for their help with cell sorting; K Burling and the MRC MDU Mouse Biochemistry Laboratory [MRC_MC_UU_12012/5] for processing mouse serum samples; R El-Khairi for her help with IF images, R Grandy for their help with providing relevant references, the Cambridge Biorepository for Translational Medicine for the provision of human tissue used in the study and Mr B McLeod for IT support. The monoclonal antibody TROMA-III developed by R Kemler was obtained from the Developmental Studies Hybridoma Bank, created by the NICHD of the NIH and maintained at The University of Iowa, Department of Biology, Iowa City, IA 52242.

Author Contributions F.S. conceived and designed the study, performed experiments, acquired, interpreted and analyzed the data, developed and validated the protocols described, generated the figures and wrote and edited the manuscript. A.W.J generated the densified collagen tubular scaffolds and conceived and developed the manufacturing technique. O.C.T. contributed to cell culture and performed animal experiments including kidney capsule injections, provision and harvesting of mouse tissue. St.S. performed the Magnetic Resonance Imaging (MRI) experiments. E.M.G. and S.S.U. reviewed and reported the MRI images. R.L.G. performed experiments including animal experiments, IF, and tissue histology. M.C.D.B. contributed to cell culture, generated viral particles, performed viral transduction experiments and generated GFP-ECOs. N.L.B. and La.V. performed animal experiments. M.J.G.-V. and P.M. performed bioinformatics analyses. D.O. performed flow cytometry analyses; L.Y. performed Western blot analyses. A.R. performed IF and QPCR analyses and provided positive controls for IF and QPCR. A.B. performed flow cytometry analyses and provided bioinformatics support. J.B. contributed to tissue histology and IF experiments. M.C.F.Z. contributed to the PGA scaffold preparation and population with cells. M.T.P. generated viral particles, performed viral transduction experiments and generated GFP-ECOs. M.P. generated viral particles. G.M.S. contributed to the scaffold generation. P.M.M. and K.E.S. maintained and provided fibroblast controls. N.P. contributed to tissue culture. N.G. and C.A.R contributed to harvesting and provision of primary tissue. I.S. performed the karyotyping and CGH analyses. S. E. D. reviewed and reported

the histology images. W.S., J.C., K.B.J., Mat.Z., Sa.S., W.T.H.G., G.J.A., S.E.B., T.A.W., T.H.K., E.M. contributed through critical revision of the manuscript for important intellectual content. N.R.F.H. contributed to the design and concept of the study and provided early study supervision. A.E.M. contributed to the design of the densified collagen scaffold and contributed through critical revision of the manuscript for important intellectual content. K.S.-P. provided primary tissue, performed animal experiments, including biliary reconstruction surgery, contributed to the design and concept of study, supervised the study, interpretated the data, wrote and edited the manuscript. L.V. Designed and conceived the study, supervised the study, interpreted the data, wrote and edited the manuscript. All the authors approved the manuscript.

Conflict of financial interests statement: LV is a founder and shareholder of DefiniGEN. The remaining authors have nothing to disclose.

References

1. Murray, K. F. & Carithers, R. L. AASLD practice guidelines: Evaluation of the patient for liver transplantation. *Hepatology* **41,** 1407–1432 (2005).

2. Perkins, J. D. Are we reporting the same thing?: Comments. *Liver Transplant.* **13,** 465–466 (2007).

3. Skaro, A. I. *et al.* The impact of ischemic cholangiopathy in liver transplantation using donors after cardiac death: The untold story. *Surgery* **146,** 543–553 (2009).

4. Enestvedt, C. K. *et al.* Biliary complications adversely affect patient and graft survival after liver retransplantation. *Liver Transpl.* **19,** 965–72 (2013).

5. Gallo, A. & Esquivel, C. O. Current options for management of biliary atresia. *Pediatr. Transplant.* **17,** 95–98 (2013).

6. Felder, S. I. *et al.* Hepaticojejunostomy using short-limb Roux-en-Y reconstruction. *JAMA Surg* **148,** 253–7-8 (2013).

7. Sampaziotis, F., Segeritz, C.-P. & Vallier, L. Potential of human induced pluripotent stem cells in studies of liver disease. *Hepatology* **62,** 303–311 (2015).

8. Kanno, N., LeSage, G., Glaser, S., Alvaro, D. & Alpini, G. Functional heterogeneity of the intrahepatic biliary epithelium. *Hepatology* **31,** 555–61 (2000).

9. Sampaziotis, F. *et al.* Cholangiocytes derived from human induced

549 pluripotent stem cells for disease modeling and drug validation. *Nat.*
550 *Biotechnol.* 1–11 (2015). doi:10.1038/nbt.3275

551 10. Sampaziotis, F. *et al.* Directed differentiation of human induced
552 pluripotent stem cells into functional cholangiocyte-like cells. *Nat.*
553 *Protoc.* **12,** 814–827 (2017).

554 11. LeSage, G., Glaser, S. & Alpini, G. Regulation of cholangiocyte
555 proliferation. *Liver* **21,** 73–80 (2001).

556 12. Huch, M. *et al.* Long-Term Culture of Genome-Stable Bipotent Stem
557 Cells from Adult Human Liver. *Cell* **160,** 299–312 (2014).

558 13. Masyuk, A. I., Masyuk, T. V & LaRusso, N. F. Cholangiocyte primary
559 cilia in liver health and disease. *Dev. Dyn.* **237,** 2007–12 (2008).

560 14. Tabibian, J. H., Masyuk, A. I., Masyuk, T. V., O'Hara, S. P. & LaRusso,
561 N. F. Physiology of cholangiocytes. *Compr. Physiol.* **3,** 541–565 (2013).

562 15. Cízková, D., Morký, J., Micuda, S., Osterreicher, J. & Martínková, J.
563 Expression of MRP2 and MDR1 transporters and other hepatic markers
564 in rat and human liver and in WRL 68 cell line. *Physiol. Res.* **54,** 419–28
565 (2005).

566 16. Gigliozzi, A. *et al.* Molecular identification and functional
567 characterization of Mdr1a in rat cholangiocytes. *Gastroenterology* **119,**
568 1113–22 (2000).

569 17. Xia, X., Francis, H., Glaser, S., Alpini, G. & LeSage, G. Bile acid
570 interactions with cholangiocytes. *World J. Gastroenterol.* **12,** 3553–63
571 (2006).

572 18. Caperna, T. J., Blomberg, L. A., Garrett, W. M. & Talbot, N. C. Culture
573 of porcine hepatocytes or bile duct epithelial cells by inductive serum-
574 free media. *In Vitro Cell. Dev. Biol. Anim.* **47,** 218–33 (2011).

575 19. Marinelli, R. A. *et al.* Secretin induces the apical insertion of aquaporin-
576 1 water channels in rat cholangiocytes. *Am. J. Physiol.* **276,** G280-6
577 (1999).

578 20. Gong, A.-Y. *et al.* Somatostatin stimulates ductal bile absorption and
579 inhibits ductal bile secretion in mice via SSTR2 on cholangiocytes. *Am.*
580 *J. Physiol. Cell Physiol.* **284,** C1205-14 (2003).

581 21. Ito, M. *et al.* NOD/SCID/gamma(c)(null) mouse: an excellent recipient
582 mouse model for engraftment of human cells. *Blood* **100,** 3175–82
583 (2002).

584 22. Chan, B. P. & Leong, K. W. Scaffolding in tissue engineering: general
585 approaches and tissue-specific considerations. *Eur. Spine J.* **17,** 467–
586 479 (2008).

587 23. Cheung, H.-Y., Lau, K.-T., Lu, T.-P. & Hui, D. A critical review on
588 polymer-based bio-engineered materials for scaffold development.
589 *Compos. Part B Eng.* **38,** 291–300 (2007).

590 24. Jabłonska, B. End-to-end ductal anastomosis in biliary reconstruction:
591 indications and limitations. *Can. J. Surg.* **57,** 271–277 (2014).

592 25. Gjorevski, N. *et al.* Designer matrices for intestinal stem cell and
593 organoid culture. *Nature* **539,** 560–564 (2016).

594 26. Koo, B. K. & Clevers, H. Stem cells marked by the r-spondin receptor

LGR5. *Gastroenterology* **147,** 289–302 (2014).

27. Farin, H. F., Van Es, J. H. & Clevers, H. Redundant sources of Wnt regulate intestinal stem cells and promote formation of paneth cells. *Gastroenterology* **143,** 1518–1529.e7 (2012).

Figure Legends

Figure 1 Derivation and characterization of Extrahepatic Cholangiocyte Organoids (ECOs). **(a)** Schematic representation of the method used for the derivation of ECOs. **(b)** Quantitative real time PCR (QPCR) confirming the expression of biliary markers in Passage 1 (P1), Passage 10 (P10) and Passage 20 (P20) ECOs compared to freshly isolated Primary Cholangiocytes (PC) and Embryonic Stem (ES) cells used as a negative control, *n* = 4 ECO lines. Center line, median; box, interquartile range (IQR); whiskers, range (minimum to maximum). Values are relative to the housekeeping gene Hydroxymethylbilane Synthase (*HMBS*) **(c)** Immunofluorescence (IF) analyses confirming the expression of biliary markers in ECO organoids. Scale bars, 100 μm. Single channel and higher magnification images are provided in **Supplementary Fig 3**. **(d)** Euclidean hierarchical clustering analysis comparing the transcriptome of primary cholangiocytes (Primary), passage 20 ECOs (ECO), hIPSC-derived intrahepatic cholangiocyte-like-cells (iChoLC), ES cells (ES) and hepatocytes (HEP). For each probe, standard scores (z-scores) indicate the differential expression measured in number of standard deviations from the average level across all the samples. Clusters of genes expressed in ECOs, primary cholangiocytes or both cell types are indicated. GO analyses for each cluster are provided in **Supplementary Fig. 7e**. The data corresponds to 3 ECO lines.

Figure 2 Functional characterization of ECO organoids. **(a)** Fluorescence images demonstrating secretion of the MDR1 fluorescent substrate rhodamine 123 in the lumen of ECOs, which is inhibited by the MDR1 inhibitor verapamil. Scale bars, 100 μm. **(b)** Fluorescence intensity along the white line in **a**. **(c)** Mean intraluminal fluorescence intensity normalized to background in freshly plated Primary Cholangiocytes (Rho PC), Passage 20 ECOs (Rho P20) and P20 ECOs treated with verapamil (Ver). Error bars, Standard Deviation (SD); n = 1565 measurements in total. ****P < 0.001, Kruskal-Wallis test with Dunn's correction for multiple comparisons. **(d)** Luminal extrusion of the fluorescent bile acid CLF compared to controls loaded with FITC, confirming bile acid transfer. Scale bars, 100 μm. **(e)** Fluorescence intensity along the white line in **d**. **(f)** Mean intra-luminal fluorescence intensity normalized over background, n = 1947 total measurements. Error bars, SD; ****P < 0.001, Kruskal-Wallis test with Dunn's correction for multiple comparisons. **(g)** ALP staining of ECOs. Scale bars, 500 μm (left) and 1 cm (right). **(h)** Mean GGT activity of P20 ECOs vs. PCs; error bars, SD; n = 3; ****P < 0.001, one-way ANOVA with Dunnett's correction for multiple comparisons. **(i,j)** Mean diameter measurements **(i)** and live images **(j)** of ECOs treated with secretin or secretin and somatostatin, n = 8. Error bars, SD; ***P < 0.001; #P > 0.05 (Kruskal-Wallis test with Dunn's correction for multiple comparisons). **(a-j)** Data representative of 3 different experiments.

Figure 3 ECOs dissociated to single cells (ECO-SCs) can populate biodegradable PGA scaffolds. **(a**,**b)** Photographs of a PGA scaffold before **(a)** and after **(b)** treatment with ECOs. Scale bars, 1 cm. **(c)** Light microscopy

images of a PGA scaffold populated with ECO-SCs. Red arrowheads: Fully populated scaffold; black arrowheads: cells recruiting new PGA fibers; white arrowheads: PGA fibers. Scale bars, 100 μm. **(d)** Confocal microscopy images demonstrating cell expansion at different time-points after seeding of GFP-positive ECO-SCs on a PGA scaffold. White lines indicate the position of PGA fibers. Scale bars, 100 μm. **(e)** IF demonstrating the expression of biliary markers and lack of EMT markers in ECO-SCs seeded on PGA scaffolds. Scale bars, 100 μm **(f)** QPCR analyses demonstrating the expression of biliary markers in ECOs before (ECOs) and after (scaffold) seeding on PGA scaffolds, n = 4 ECO lines. Center line, median; box, interquartile range (IQR); whiskers, range (minimum to maximum). Values are relative to the housekeeping gene *HMBS*. **(g)** Mean ratio of CK7+/CK19+ and CK19+/Vimentin (VIM)+ cells in IF analyses similar to the image shown in **(e)**. Error bars represent SD; n = 6. $^{**}P < 0.01$ (Mann-Whitney test). **(h)** Mean GGT activity of ECO-SCs populating a PGA scaffold, n = 4. Error bars represent SD. $^{****}P < 0.001$ (two-tailed Student's t-test). **(i)** ALP staining of PGA scaffolds populated by ECO-SCs. Scale bars, 500 μm.

Figure 4 Biliary reconstruction in an extrahepatic biliary injury (EHBI) mouse model using ECOs. **(a)** Schematic representation of the method used for biliary reconstruction. **(b)** Kaplan–Meier survival analysis, demonstrating rescue of EHBI mice following biliary reconstruction with ECO-populated scaffolds. $^{**}P < 0.01$ (log-rank test). **(c)** Images of gallbladders reconstructed with acellular PGA scaffolds (scaffold only), PGA scaffolds populated with ECOs (transplanted) and native un-reconstructed gallbladder controls (not

transplanted), demonstrating full reconstruction with ECO populated scaffolds. CD: cystic duct, CBD: common bile duct, CHD: common hepatic duct, F: fundus, A: anterior surface, P: posterior surface. Scale bars, 500 μm. **(d)** H&E staining of the reconstructed gallbladders. L: lumen. Scale bars, 100 μm **(e)** IF analyses demonstrating the presence of GFP-positive ECOs expressing biliary markers in the reconstructed gallbladders. L: lumen Scale bars, 100 μm. Higher magnification images are provided in **Supplementary Fig. 12 (f**,**g)** FITC cholangiogram (*n* = 1) **(f)** and MRCP images (*n* = 2) **(g)** of reconstructed (transplanted) vs. native control (not transplanted) gallbladders (GB) demonstrating a patent lumen and unobstructed communication with the rest of the biliary tree. Scale bars, 1 mm **(f)**, 5 mm **(g)**.

Figure 5 ECOs can populate densified collagen tubular scaffolds. **(a)** Schematic representation of the method used for the generation of densified collagen tubular scaffolds. **(b)** Image of a densified collagen construct prior to tube excision. Scale bar, 500 μm. **(c)** Maximum intensity projection image demonstrating a GFP+ ECO-populated tube after its generation. Scale bar, 30 μm **(d)** Confocal microscopy image demonstrating lumen patency of an ECO-populated collagen tube. Scale bar, 30 μm. **(e)** Images of a near confluent GFP+ ECO-tube. Scale bar; 100 μm. **(f)** IF analyses demonstrating the expression of biliary markers by ECOs following the generation of ECO-tubes. Scale bar, 100 μm. **(g)** QPCR analyses demonstrating the expression of biliary markers before (ECOs) and after (Scaffold) the generation of ECO-populated collagen tubes. ES cells are used as a negative control, *n* = 4 ECO

lines. Center line, median; box, interquartile range (IQR); whiskers, range (minimum to maximum). Values are relative to *HMBS* expression. **(h**,**i)** ECO-tubes exhibit ALP **(h)** and GGT **(i)** activity. Scale bars, 500μm; MEFs, Mouse Embryonic feeders used as negative control; Scaffold, ECO-populated, densified collagen tubes; error bars, SD; *n* = 3.

Figure 6 Bile duct replacement using ECO-populated densified collagen tubes. **(a)** Schematic representation of the method used. **(b)** Postmortem images of mice receiving ECO-populated collagen tubes (ECOs) vs. mice receiving fibroblast-populated tubes (fibroblasts). Bile flow results in yellow pigmentation of ECO-tubes. The white color of the fibroblast conduit combined with a dilated bile-filled (yellow color) proximal bile duct (PBD) suggests luminal occlusion, resulting in bile leak (yellow peritoneal pigmentation; white dashed line). SC: Collagen tubes/scaffolds; DBD: Distal Bile Duct; scale bars, 500 μm. **(c)** Images of a thin walled construct resembling the native bile duct in animals receiving ECO-populated tubes vs. a thickened construct with no distinguishable lumen in animals receiving fibroblast tubes. Scale bars, 500 μm. **(d)** QPCR using human-specific primers confirming the expression of biliary markers by transplanted ECO-populated tubes (ECOs *in vivo*) compared to cultured ECOs (ECOs *in vitro*) and mouse biliary tissue used as a negative control, *n* = 4. Center line, median; box, interquartile range (IQR); whiskers, range (minimum to maximum). Values are relative to *HMBS* expression. **(e)** H&E staining demonstrating the presence of a biliary epithelium and a patent lumen in ECO-tubes but not fibroblast constructs. Scale bars, 100 μm. **(f)** IF analyses demonstrating a GFP+/

CK19+ epithelium lining the lumen of ECO-constructs, vs. obliteration of the lumen by fibroblasts in fibroblast constructs. Scale bars, 100 μm. **(g)** FITC cholangiogram, demonstrating lumen patency in ECO-tubes vs. lumen occlusion in fibro-constructs. Scale bars, 100 μm (ECO) and 500 μm (Fibroblasts**) (h)** ALP activity is observed only in ECO-tubes, but not in fibroblast constructs. Scale bars, 100 μm (ECO) and 500 μm (Fibroblasts**).**

Online Methods

Primary biliary tissue

Primary biliary tissue (bile duct or gallbladder) was obtained from deceased organ donors from whom organs were being retrieved for transplantation. The gallbladder or a section of the bile duct was excised during the organ retrieval operation after obtaining informed consent from the donor's family (REC reference numbers: 12/EE/0253, NRES Committee East of England - Cambridge Central and 15/EE/0152 NRES Committee East of England - Cambridge South).

Isolation of primary cholangiocytes

Excised bile duct segments were placed in a 10 cm plate and washed once with William's E medium (Gibco, Life Technologies). A longitudinal incision was made along the wall of the excised bile duct segment exposing the lumen and 10-15 ml of William's E medium were added to cover the tissue. The luminal epithelium was subsequently scraped off using a surgical blade, while submerged in medium. The supernatant was collected and the tissue and plate were washed 2-3 times with William's E medium to harvest any remaining cells. The supernatant and washes were centrifuged at 444g for 4 minutes. The pellet was washed with William's E, re-centrifuged and the supernatant was discarded (**Fig. 1a**).

Excised gallbladders were placed in a 15 cm plate, a longitudinal incision was made along the wall of the excised gallbladder and the lumen was washed once with William's E medium (Gibco, Life Technologies). Cholangiocytes

were isolated and harvested following the method described above (**Supplementary Fig. 2a**).

For isolation through brushings, an excised bile duct segment was placed in a 10 cm plate and cannulated using an ERCP brush. The lumen was brushed 10-20 times and the cells were harvested by washing the brush several times in a falcon tube containing 40-50 ml of William's E medium (**Supplementary Fig. 2b**).

Generation and culture of ECOs

Isolated primary cholangiocytes were centrifuged at 444g for 4 minutes and re-suspended in a mixture of 66% matrigel (BD Biosciences, catalogue number: 356237) and 33% William's E medium (Gibco, Life Technologies) supplemented with 10mM nicotinamide (Sigma-Aldrich), 17mM sodium bicarbonate (Sigma Aldrich), 0.2mM 2-Phospho-L-ascorbic acid trisodium salt (Sigma-Aldrich), 6.3mM sodium pyruvate (Invitrogen), 14mM glucose (Sigma-Aldrich), 20mM HEPES (Invitrogen), ITS+ premix (BD Biosciences), 0.1μM dexamethasone (R&D Systems), 2mM Glutamax (Invitrogen),100U/ml penicillin per 100μg/ml streptomycin, 20ng/ml EGF (R&D Systems), 500ng/ml R-Spondin (R&D Systems) and 100ng/ml DKK-1 (R&D Systems). The cell suspension was plated in 24-well plate format, at 50μl/well, so that a small dome of matrigel was formed in the centre of each well and then incubated at 37^{o}C for 10-30 minutes until it solidified. Subsequently, 1ml of William's E medium with supplements was added. The culture medium was changed every 48 hours.

To split the cells, the matrigel was digested by adding Cell Recovery Solution (Corning) for 30 minutes at 4^{o}C. The resulting cell suspension was harvested, centrifuged at 444g for 4 minutes, washed once with William's E medium and re-suspended in 66% matrigel and 33% William's E medium with supplements, as described above.

All experiments were performed using passage 20 ECOs unless otherwise stated.

Cell line identity

Demographic data for donor corresponding to the each ECO lines is provided in supplementary table 1. Following derivation ECO lines were authenticated by matching their karyotype (**Supplementary Fig. 4b**) to the sex of the donor of origin. The lines were tested on a regular basis and found to be negative for mycoplasma contamination.

Immunofluorescence, RNA extraction and Quantitative Real Time PCR

IF, RNA extraction and QPCR were performed as previously described[9]. A complete list of the primary and secondary antibodies used is provided in supplementary table 3. A complete list of the primers used is provided in supplementary table 4.

All QPCR data are presented as the median, interquartile range (IQR) and range (minimum to maximum) of four independent ECO lines unless otherwise stated. Values are relative to the housekeeping gene Hydroxymethylbilane Synthase (*HMBS*).

All IF images were acquired using a Zeiss Axiovert 200M inverted microscope or a Zeiss LSM 700 confocal microscope. Imagej 1.48k software (Wayne

799 Rasband, NIHR, USA, http://imagej.nih.gov/ij) was used for image processing.
800 IF images are representative of 3 different experiments. IF images of
801 reconstructed gallbladder sections are representative of 5 different animals.

802 **Microarrays**

863 RNA for microarray analysis was collected from 3 different ECO lines (n=3).
864 The RNA was assessed for concentration and quality using a SpectroStar
865 (BMG Labtech, Aylesbury, UK) and a Bioanalyser (Agilent Technologies,
866 Cheadle, UK). Microarray experiments were performed at Cambridge
867 Genomic Services, University of Cambridge, using the HumanHT-12 v4
868 Expression BeadChip (Illumina, Chesterford, UK) according to the
869 manufacturer's instructions. Briefly, 200ng of Total RNA underwent linear
870 amplification using the Illumina TotalPrep RNA Amplification Kit (Life
871 Technologies, Paisley, UK) following the manufacturer's instructions. The
872 concentration, purity and integrity of the resulting cRNA were measured by
873 SpectroStar and Bioanalyser. Finally cRNA was hybridised to the HumanHT-
874 12 v4 BeadChip overnight followed by washing, staining and scanning using
875 the Bead Array Reader (Illumina). The microarray data are available on
876 ArrayExpress (Accession number: E-MTAB-4591).

877 **Microarrays analysis**

878 Raw data was loaded into R using the lumi package from bioconductor[28] and
879 divided into subsets according to the groups being compared; only the
880 samples involved in a given comparison are used. Subsets were then filtered
881 to remove any non-expressed probes using the detection p-value from
882 Illumina. Across all samples probes for which the intensity values were not
883 statistically significantly different ($P > 0.01$) from the negative controls were

884 removed from the analysis. Following filtering the data was transformed using
885 the Variance Stabilization Transformation[29] from lumi and then normalised to
886 remove technical variation between arrays using quantile normalisation.
887 Comparisons were performed using the limma package[30] with results
888 corrected for multiple testing using False Discovery Rate (FDR) correction.
889 Finally the quality of the data was assessed along with the correlations
890 between samples within groups.
891 Probes differentially expressed between HEP and ECOs representing the
892 aggregate transcriptional "signature" of ECOs were selected for Euclidean
893 hierarchical clustering using Perseus software (MaxQuant). Standard scores
894 (z-scores) of the log2 normalized probe expression values across the different
895 conditions were calculated and used for this analysis. Heatmaps and Primary
896 Component Analysis (PCA) plots were generated using the MaxQuant
897 Perseus software (http://www.perseus-framework.org/)[31]. Functional
898 annotation and gene ontology analyses were performed on the genes
899 differentially expressed between PCs and ECOs (Figure 1d) using the
900 NIAID/NIH Database for Annotation, Visualization and Integrated Discovery
901 (DAVID) v6.8 (https://david.ncifcrf.gov/)[32,33].
902 **Western Analysis**
903 Total protein was extracted with lysis buffer (50mM Tris pH 8, 150mM NaCl,
904 0.1% SDS, 0.5% sodium deoxycholate, 1% Trition X-100 and protease and
905 phosphatase inhibitors). Protein concentrations were determined by BCA
906 Protein Assay Kit (Thermo Fisher Scientific) according to the manufacturer's
907 instructions. Samples were prepared for Western blot by adding 1x NuPAGE
908 LDS Sample Buffer with 1% β-mercaptoethanol and incubated for 5 minutes

at 95°C. Protein (25 µg) was separated by 4-12% NuPAGE Bis-Tris protein gels (Invitrogen) and transferred onto PVDF membranes (Bio-Rad). Proteins were detected by probing with antibodies specific to Phospho-β-catenin (Ser33/37/Thr41) (Cell Signalling Technology), Active-β-catenin (Millipore), Total-β-catenin (R&D), α-tubulin (Sigma) followed by incubation with horseradish peroxidase anti-mouse, anti-goat or anti-rabbit secondary antibodies. Membranes were developed using Pierce ECL Western blotting substrate (Thermo Scientific) according to the manufacturer's instructions. The raw Western Blot images are provided in **Supplementary Fig. 14**.

Rho Kinase activity analyses

Rho Kinase activity was measured using a commercially available kit (Cell Biolabs, STA-416) according to the manufacturer's instructions

Flow cytometry analyses

ECO organoids were harvested using Cell Recovery Solution (Corning) for 30 minutes at 4^{o}C, centrifuged at 444g for 4 minutes and dissociated to single cells using TrypLE^{TM} Express (Gibco). The cells were subsequently fixed using 4% PFA for 20 minutes at 4^{o}C. Cell staining and flow cytometry analyses were performed as previously described[9,34].

Karyotyping

ECO organoids were harvested using Cell Recovery Solution (Corning), dissociated to single cells as described above, plated in gelatin coated plates and cultured using William's E medium with supplements. When the cells were sub-confluent, usually after 72hrs, the cultures were incubated for 3-4 hours with William's E medium with supplements containing 0.1µg/ml colcemid (Karyomax®, Gibco). The cells were then harvested using Trypsin-

EDTA (0.05%) (Gibco) for 4-5 minutes at 37°C, centrifuged at 344g for 5 minutes and re-suspended in 5mls of KCl hypotonic solution (0.055M). The suspension was re-centrifuged at 344g for 5 minutes, 2 mls of a 3:1 100% methanol:glacial acetic acid solution were added and slides were prepared as previously described[35]

Comparative Genomic Hybridization analyses

Genomic DNA was labeled using the BioPrime DNA Labeling Kit (Invitrogen), according to the manufacturer's instructions and samples were hybridised to Agilent Sureprint G3 unrestricted CGH ISCA 8x60K human genome arrays following the manufacturer's protocol, as previously described[36]. The data was analysed using the Agilent CytoGenomics Software.

Rhodamine123 transport assay

The Rhodamine 123 transport assay was performed as previously described[9] and images were acquired using a Zeiss LSM 700 confocal microscope. Fluorescence intensity was measured between the organoid interior and exterior and luminal fluorescence was normalized over the background of the extraluminal space. Each experiment was repeated in triplicate. Error bars represent SD.

Cholyl-Lysyl-Fluorescein transport assay

To achieve loading with Cholyl-Lysyl-Fluorescein (CLF, Corning Incorporated), ECO organoids were split in 5μM of CLF and incubated at 37°C for 30 minutes. Images were acquired using a Zeiss LSM 700 confocal microscope and fluorescence intensity was measured between the organoid interior and exterior as described for the Rhodamine 123 transport assay. To demonstrate that the changes in CLF fluorescence intensity observed were

959 secondary to active export of CLF from the organoid lumen, the experiment
960 was repeated with 5μM of unconjucated Fluorescein Isothiocyanate (FITC)
961 (Sigma-Aldrich) as a control. Fluorescence intensity measurements were
962 performed as described for the Rhodamine 123 transport assay. Each
963 experiment was repeated in triplicate. Error bars represent SD.

964 **GGT activity**

965 GGT activity was measured in triplicate using the MaxDiscovery™ gamma-
966 Glutamyl Transferase (GGT) Enzymatic Assay Kit (Bioo scientific) based on
967 the manufacturer's instructions. Error bars represent SD.

968 **Alkaline Phosphatase staining**

969 Alkaline phosphatase was carried out using the BCIP/NBT Color
970 Development Substrate (5-bromo-4-chloro-3-indolyl-phosphate/nitro blue
971 tetrazolium) (Promega) according to the manufacturer's instructions.

972 **Response to Secretin and Somatostatin**

973 Responses to secretin and somatostatin were assessed as previously
974 described[9].

975 **Generation of ECOs expressing Green Fluorescent Protein**

976 EGFP expressing VSV-G pseudotyped, recombinant HIV-1 lentiviral particles
977 were produced with an optimized second generation packaging system by
978 transient co-transfection of three plasmids into HEK 293T cells (ATCC CRL-
979 11268). EGFP expression is under control of a core EF1α-promoter. All
980 plasmids were a gift from Didier Trono and obtained from addgene (pWPT-
981 GFP #12255, psPAX2 #12260, pMD2.G, #12259). Viral infection of organoids
982 was performed as previously described[37]. Infected ECOs were expanded for 2
983 passages, harvested as described above for flow cytometry analyses and cell

sorting by flow cytometry for GFP positive cells was performed. GFP expressing single cells were plated using our standard plating method and cultured in William's E medium with supplements for 1-2 weeks until fully grown ECO organoids developed.

Generation of ECO populated PGA scaffolds

1mm thick PolyGlycolic Acid (PGA) scaffolds with a density of 50mg/cc were used for all experiments. Prior to seeding cells, the PGA scaffolds were pre-treated with a 1M NaOH for 10-30 seconds washed 3 times, decontaminated in a 70% ethanol solution for 30 minutes and then air-dried for another 30 minutes until all the ethanol had fully evaporated. All scaffolds were a gift from Dr Sanjay Sinha and obtained from Biomedical Structures (Biofelt).

ECOs were harvested and dissociated to single cells as previously described for flow cytometry analyses. 5-10x10^6 cells were re-suspended in 100 µl of William's E medium with supplements, seeded on a scaffold surface area of 1cm^2 and incubated at 37^oC for 30-60 minutes to allow the cells to attach to the scaffold. The scaffolds were placed in wells of a 24-well plate and checked at regular intervals during this period to ensure the medium did not evaporate. If necessary, 10-20 µl of William's E medium with supplements were added. After 1 hour, 2-3 mls of William's E medium with supplements were added to the wells and the medium was changed twice weekly.

Generation of densified collagen tubes

Densified collagen tubes were prepared using a novel approach. A 3D printed chamber was fabricated, consisting of a funnel piece and a base plate. A 250µm thick metallic wire was mounted into the base plate and fed through the centre of the funnel. Absorbent paper towels were compacted between

1009 the two 3D printed parts, which were then screwed together. 5 mg mL^{-1}
1010 collagen gel solution, loaded with cells, was poured into the funnel and gelled
1011 at 37ºC for 30 min. After that time, the screws were loosened and, by placing
1012 the 3D printed chambers at 37ºC for 2-4h, water was drawn out of the
1013 collagen gel. A cell-loaded densified collagen tube was thus formed with a
1014 250μm lumen and a wall thickness of 30-100 μm, determined by the duration
1015 of the drying phase. Upon removal from the chamber, the tube was trimmed
1016 for excess collagen and cut to the required length.

1017 **Culture of Human Mammary Epithelial Cells (HMECs)**

1018 HMECs and the required tissue culture consumables were purchased as a kit
1019 from Lonza (cat no. cat no. CC-2551B) and the cells were cultured according
1020 to the supplier's instructions

1021 **Animal experiments**

1022 All animal experiments were performed in accordance with UK Home Office
1023 regulations (UK Home Office Project License numbers PPL 80/2638 and PPL
1024 70/8702). Immunodeficient NOD.Cg-Prkdc^{scid} Il2rg^{tm1Wjl}/SzJ (NSG) mice which
1025 lack B, T and NK lymphocytes[38] were bred in-house with food and water
1026 available ad libitum pre- and post-procedures. A mix of male and female
1027 animals were used, aged approximately 6-8 weeks. All the ECO-constructs
1028 used were populated with ECOs derived from the common bile duct.

1029 **Generation of Extra-Hepatic Biliary Injury (EHBI) mouse model**

1030 To generate a model of extrahepatic biliary injury, midline laparotomy was
1031 performed and the gallbladder was first mobilized by dividing the ligamentous
1032 attachment connecting its fundus to the anterior abdominal wall under
1033 isoflurane general anesthesia. A longitudinal incision was then made along

2/3 of the length of the gallbladder, from the fundus towards Hartmann's pouch (neck of gallbladder).

Biliary reconstruction in EHBI mice

To reconstruct the gallbladder, a scaffold section measuring approximately 1 x 1 mm (seeded with ECOs or without ECOs in controls) was sutured as a 'patch' to close the defect using 4 – 6 interrupted 10'0 non-absorbable nylon sutures under 40x magnification. The laparotomy was closed in two layers with continuous 5'0 absorbable Vicryl sutures. The animals were given buprenorphine (temgesic 0.1 mg/kg) analgesia as a bolus and observed every 15 minutes in individual cages until fully recovered.

8 animals underwent biliary reconstruction using an ECO-populated scaffold. All animals survived up to 104 days without complications and were culled electively for further analyses. Two control experiments were performed, where the animals underwent biliary reconstruction using acellular scaffolds. Both animals died within 24 hours from bile leak, therefore no further control experiments were performed to minimize animal discomfort.

Bile duct replacement

The native common bile duct was divided and a short segment excised. The populated densified collagen tube was anastomosed end-to-end, using interrupted 10'0 nylon sutures, between the divided proximal and distal common bile duct. A length of 5'0 nylon suture material (diameter 100 μm) was inserted into the collagen tube and fed into the proximal and distal common bile duct to ensure patency of the lumen during the anastomosis. After the anastomosis was complete, the 5'0 suture was pushed into the duodenum through the distal bile duct and was removed through an incision in

the duodenum, which was then closed with interrupted 10’0 nylon sutures. Lumen patency was assessed at the time of transplantation through light microscopy and cannulation of the lumen with a 5’0 non-absorbable suture. Transplantation was abandoned as futile in case of fully occluded tubes due to cell infiltration. These events were considered construct/tube failure rather than surgical complications and therefore were not censored in the survival analysis.

Bile duct ligation

C57BL/6 mice were purchased from The Jackson Laboratory (Bar Harbor, ME). The mice were housed and bred in a Minimal Disease Unit at the animal facility at Oslo University Hospital, Rikshospitalet, Oslo. All experiments were performed on male mice between 8 and 12 weeks of age. A median laparotomy was performed, the common bile duct exposed and ligated close to the junction of the hepatic bile ducts. Sham operated mice underwent the same procedure without ligation. Serum was harvested after 5 days. Alanine transaminase (ALT), aspartate transaminase (AST) and alkaline phosphatase (ALP) were measured in serum using an ADVIA 1800 (Siemens) at The Central Laboratory, Norwegian School of Veterinary Science. All animal experiments were approved by the Norwegian Food Safety Authority (project license no FOTS 8210/15) and all animals received human care in line with "Guide for the Care and Use of Laboratory Animals" (National Institutes of Health Publication, 8th Edition, 2011).

Blood sample collection

Blood was taken using a 23g needles directly from the inferior vena cava under terminal anesthesia at the time the animals were electively culled and transferred into 1.5ml Eppendorf tubes for further processing.

Blood sample processing

The blood samples were routinely processed by the University of Cambridge Core biochemical assay laboratory (CBAL). All of the sample analysis was performed on a Siemens Dimension EXL analyzer using reagents and assay protocols supplied by Siemens.

Light microscopy imaging

Light microscopy images of excised reconstructed gallbladders were acquired using a Leica MZFLIII fluorescence dissecting microscope. The images are representative of 5 animals.

Cryosectioning and Histology

Excised gallbladders were fixed in 4% PFA, immersed in sucrose solution overnight, mounted in optimal cutting temperature (OCT) compound and stored at -80°C until sectioning. Sections were cut to a thickness of 10μm using a cryostat microtome and mounted on microscopy slides for further analysis

Haematoxylin and Eosin (H&E) Staining

H&E staining was performed using Sigma-Aldrich reagents according to the manufacturer's instructions. Briefly, tissue sections were hydrated, treated with Meyer's Haematoxylin solution for 5 minutes (Sigma-Aldrich), washed with warm tap water for 15 minutes, placed in distilled water for 30-60 seconds and treated with eosin solution (Sigma-Aldrich) for 30-60 seconds.

The sections were subsequently dehydrated and mounted using the Eukitt® quick-hardening mounting medium (Sigma-Aldrich). Histology sections were reviewed by an independent histopathologist with a special interest in hepatobiliary histology (SD).

TUNEL assay

The TUNEL assay was performed using a commercially available kit (abcam, ab66110) according to the manufacturer's instructions.

Fluorescein Isothiocyanate (FITC) cholangiography

In situ FITC cholangiography was performed in sacrificed animals after dissection of the gallbladder free from the adherent liver lobes, but before surgical interruption of the extrahepatic biliary tree. The distal bile duct was cannulated with a 23½ gauge needle and FITC injected retrogradely into the gallbladder and images taken under a fluorescent microscope.

Magnetic Resonance Cholangio-Pancreatography (MRCP)

Magnetic resonance cholangio-pancreatography was performed after sacrifice of the animals. MRCP was performed at 4.7T using a Bruker BioSpec 47/40 system. A rapid acquisition with relaxation enhancement sequence was used with an echo train length of 40 echoes at 9.5ms intervals, a repetition time of 1000ms, field of view $5.84\times4.18\times4.18cm^3$ with a matrix of 256×180×180 yielding an isotropic resolution of 230 μm. The actively-decoupled four-channel mouse cardiac array provided by Bruker was used for imaging.

For the second mouse imaged, for higher signal to noise ratio to give improved visualisation of the biliary ducts a two-dimensional sequence was used with slightly varied parameters (24 spaced echoes at 11ms intervals to give an effective echo time of 110ms; repetition time 5741ms; matrix size of

256×256; field of view of 4.33×5.35cm^2 yielding a planar resolution of 170×200μm^2). Fifteen slices were acquired coronally through the liver and gall bladder with a thickness of 0.6mm. For this acquisition, a volume coil was used to reduce the impact of radiofrequency inhomogeneity.

To examine the biliary ducts and gall bladder, images were prepared by maximum intensity projections. Structural imaging to rule out neoplastic growths was performed using a T1-weighted 3D FLASH (fast low-angle shot) sequence with a flip angle of 25°, repetition time of 14ms and an echo time of 7ms. The matrix was 512×256×256 with a field of view of 5.12×2.56×2.56cm^3 for a final isotropic resolution of 100 μm.

The MRCP images were reviewed by 2 independent radiologists with a special interest in hepatobiliary radiology (EMG, SU).

Statistical analyses

All statistical analyses were performed using GraphPad Prism 6. For small sample sizes where descriptive statistics are not appropriate, individual data points were plotted. For comparison between 2 mean values a 2-sided Student's *t*-test was used to calculate statistical significance. The normal distribution of our values was confirmed using the D'Agostino & Pearson omnibus normality test where appropriate. Variance between samples was tested using the Brown-Forsythe test. For comparing multiple groups to a reference group one-way ANOVA with Dunnett correction for multiple comparisons was used between groups with equal variance, while the Kruskal-Wallis test with Dunn's correction for multiple comparisons was applied for groups with unequal variance. Survival was compared using log-rank (Mantel-Cox) tests. Where the number of replicates (*n*) is given this

refers to ECO lines or number of different animals unless otherwise stated. Further details of the statistical analyses performed are provided in **Supplementary Table 5**.

For animal experiments, group sizes were estimated based on previous study variance. Final animal group sizes were chosen to allow elective culling at different time point while maintaining $n > 4$ animals surviving past 30 days to ensure reproducibility. No statistical methods were used to calculate sample size. No formal randomization method was used to assign animals to study groups. However, littermate animals from a cage were randomly assigned to experimental or control groups by a technician not involved in the study. No animals were excluded from the analysis. No blinding was used when only one group of animals survived for radiology imaging. In cases, such as gallbladders reconstructed with fibroblasts vs. ECOs where more than one groups survived to be imaged, both radiologists reviewing the images (EG and SU) where blinded to the method of reconstruction.

References

28. Du, P., Kibbe, W. a & Lin, S. M. lumi: a pipeline for processing Illumina microarray. *Bioinformatics* **24,** 1547–8 (2008).

29. Lin, S. M., Du, P., Huber, W. & Kibbe, W. A. Model-based variance-stabilizing transformation for Illumina microarray data. *Nucleic Acids Res.* **36,** (2008).

30. Smyth, G. K. Linear models and empirical bayes methods for assessing differential expression in microarray experiments. *Stat Appl Genet Mol Biol* **3,** Article3-Article3 (2004).

31. Tyanova, S. *et al.* The Perseus computational platform for comprehensive analysis of (prote)omics data. *Nat. Methods* **13,** 731–40 (2016).

32. Huang, D. W., Sherman, B. T. & Lempicki, R. A. Systematic and integrative analysis of large gene lists using DAVID bioinformatics resources. *Nat. Protoc.* **4,** 44–57 (2008).

33. Huang, D. W., Sherman, B. T. & Lempicki, R. A. Bioinformatics enrichment tools: paths toward the comprehensive functional analysis of large gene lists. *Nucleic Acids Res.* **37,** 1–13 (2009).

34. Bertero, A. *et al.* Activin/Nodal signaling and NANOG orchestrate human embryonic stem cell fate decisions by controlling the H3K4me3 chromatin mark. *Genes Dev.* **29,** 702–17 (2015).

35. Campos, P. B., Sartore, R. C., Abdalla, S. N. & Rehen, S. K. Chromosomal spread preparation of human embryonic stem cells for

karyotyping. *J. Vis. Exp.* 4–7 (2009). doi:10.3791/1512

36. Hannan, N. R. F. *et al.* Generation of multipotent foregut stem cells from human pluripotent stem cells. *Stem Cell Reports* **1,** 293–306 (2013).

37. Koo, B.-K., Sasselli, V. & Clevers, H. Retroviral gene expression control in primary organoid cultures. *Curr. Protoc. Stem Cell Biol.* **27,** Unit 5A.6. (2013).

38. Shultz, L. D. *et al.* Human lymphoid and myeloid cell development in NOD/LtSz-scid IL2R gamma null mice engrafted with mobilized human hemopoietic stem cells. *J. Immunol.* **174,** 6477–6489 (2005).

Sampaziotis et al. Figure 1

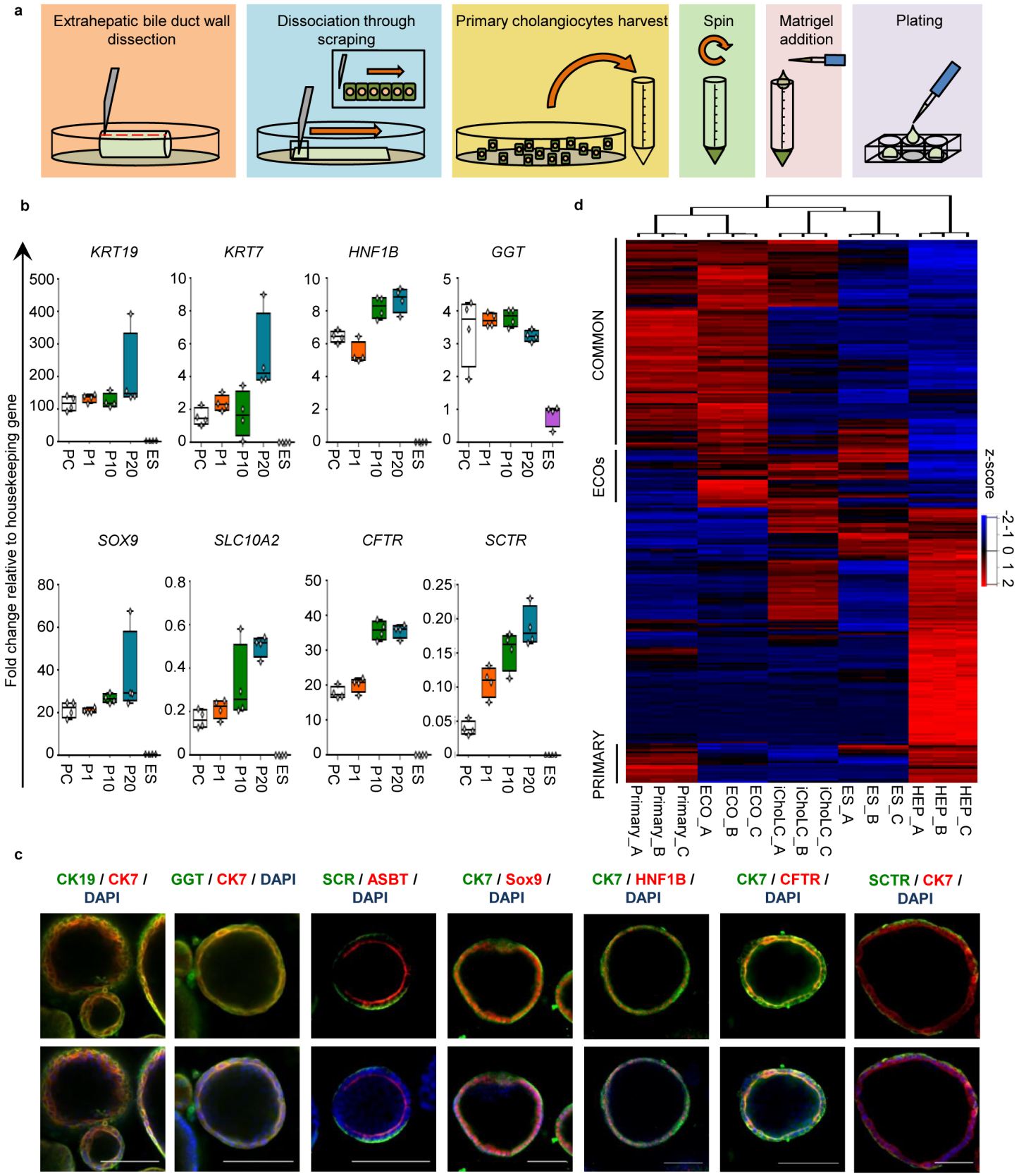

Sampaziotis et al. Figure 2

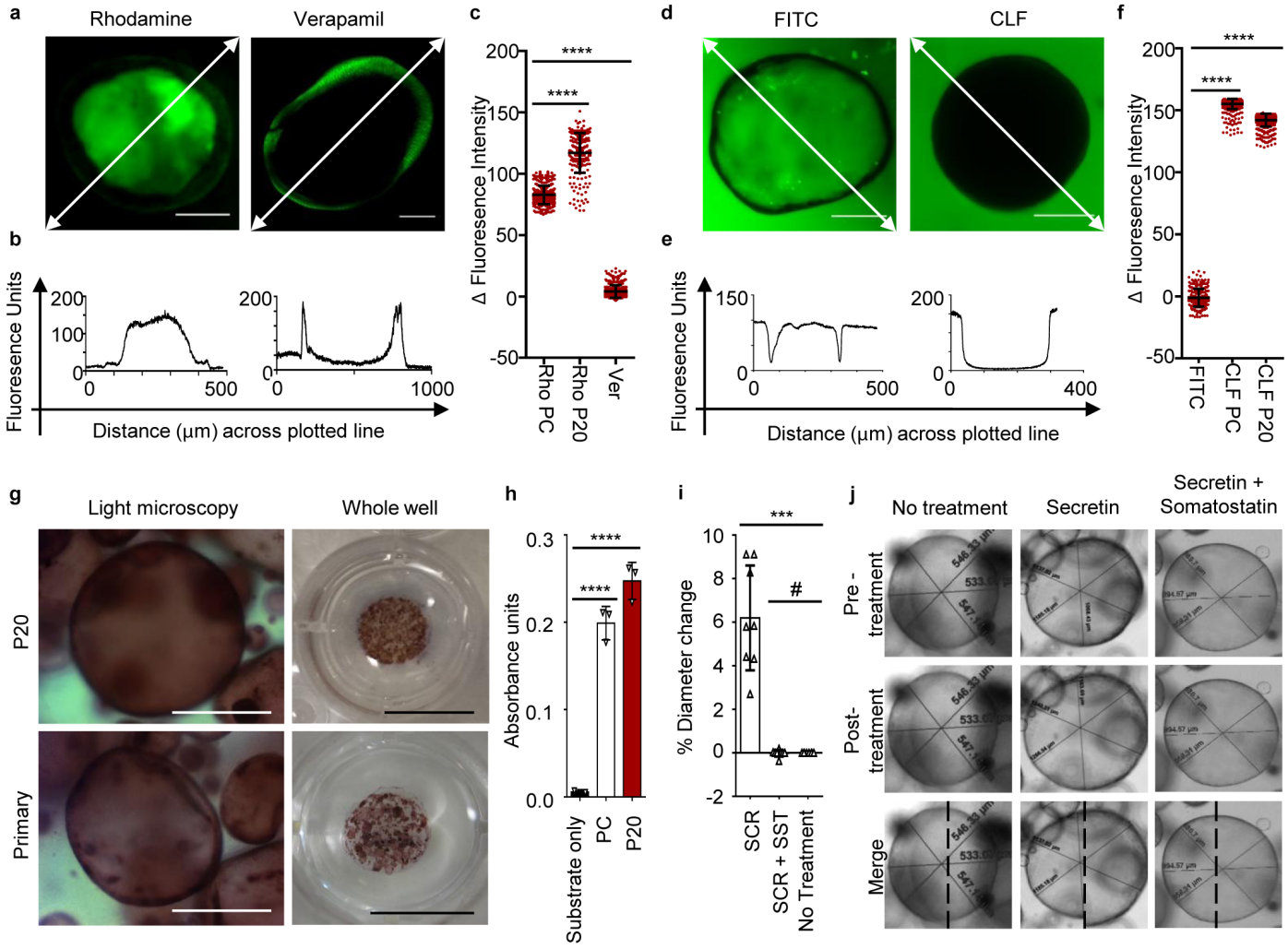

Sampaziotis et al. Figure 3

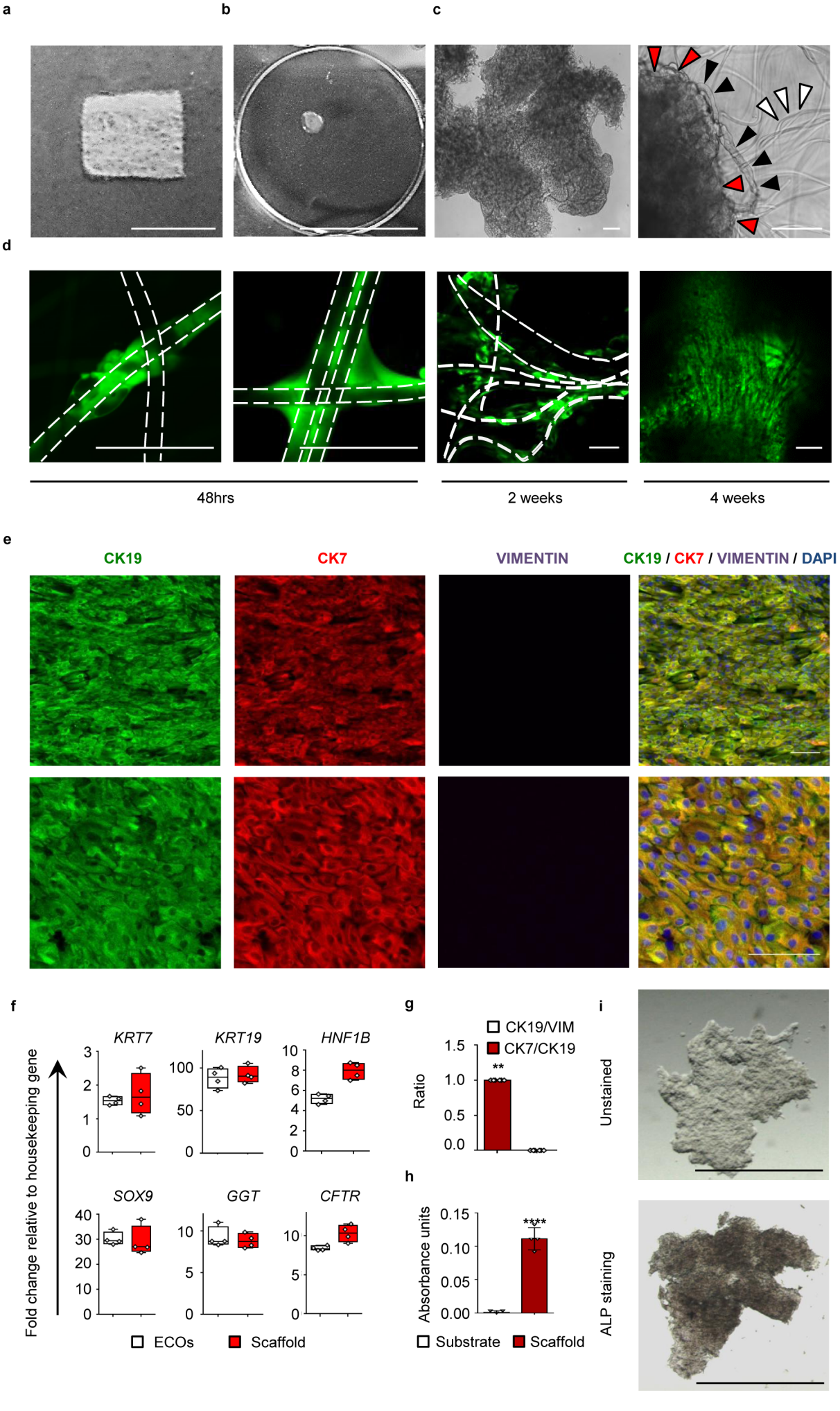

Sampaziotis et al. Figure 4

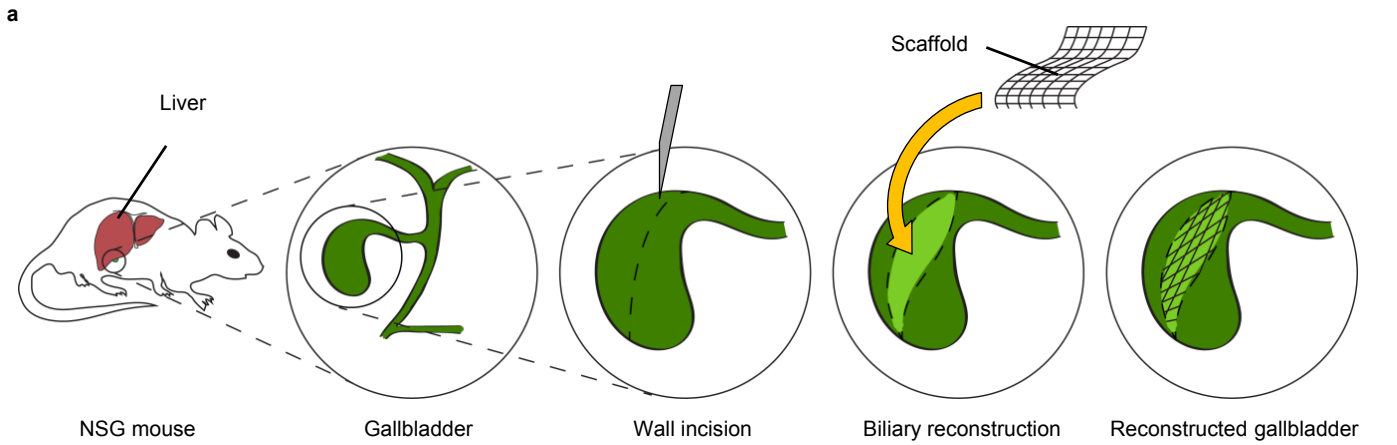

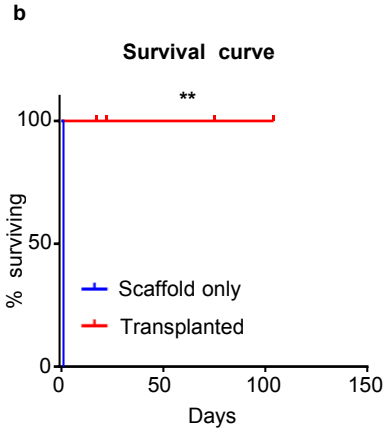

Number of mice at risk						
Days	0	1	17	22	75	104
Control	2	2	0	0	0	0
Scaffold	8	8	8	5	4	3

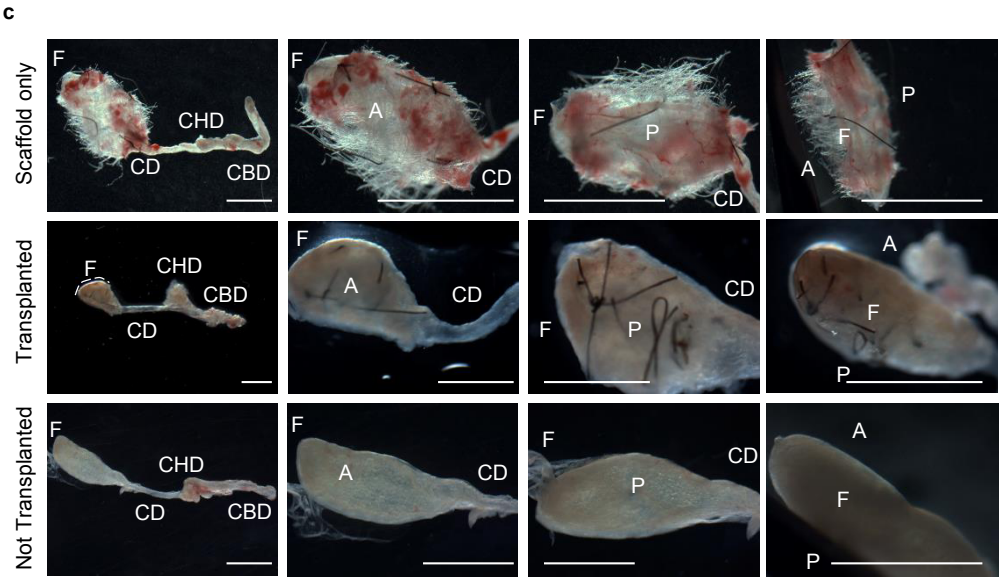

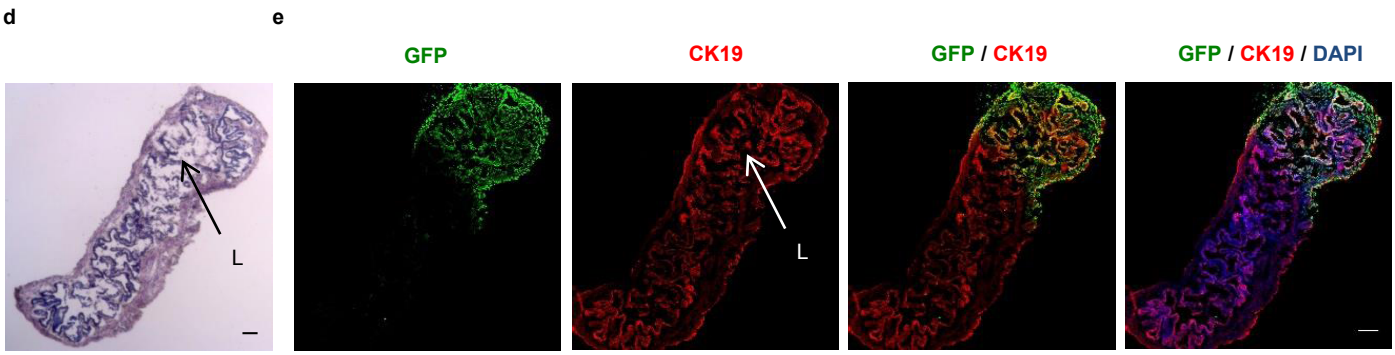

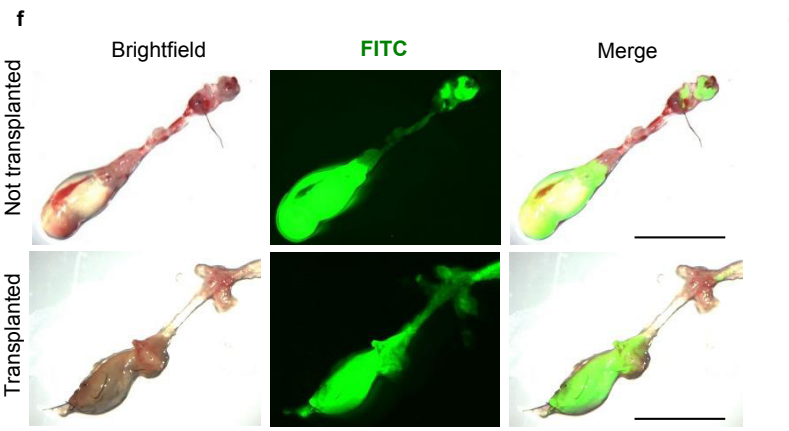

Sampaziotis et al. Figure 5

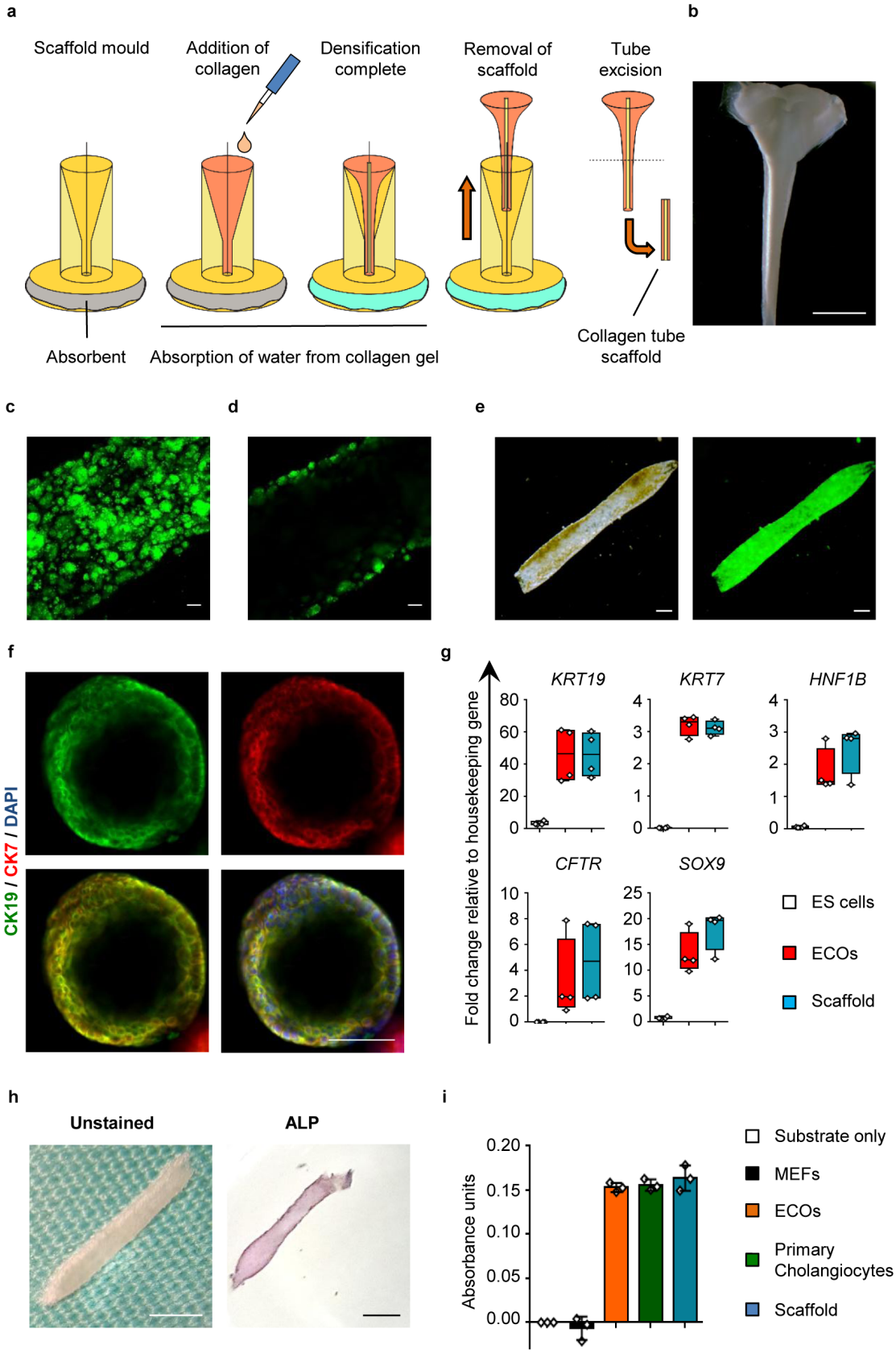

Sampaziotis et al. Figure 6